A study on additive manufacturing build parameters as bonded joint design factors

A study on Additive Manufacturing build parameters as bonded joint design factors

L. Bergonzi[a,b], A. Pirondi [a]*, F. Moroni[a], M. Frascio[c] and M. Avalle[c,d]

[a]*Dipartimento di Ingegneria e Architettura, Università di Parma, Parco Area delle Scienze 181/A, 43124 Parma, Italy*

[b]*MaCh3D srl, V.Le Duca Alessandro 42, 43123 Parma, Italy*

[c]*Dipartimento di Ingegneria Meccanica, Energetica, Gestionale e dei Trasporti, Università degli Studi di Genova, Via all'Opera Pia 15/A, 16145 Genova, Italy*

[d]*Laboratorio Congiunto Genoa Additive Manufacturing (GeAM), Via all'Opera Pia, 15/A, 16145 Genova, Italy*

Abstract

This work is aimed at exploring the influence of Fused Filament Fabrication (FFF) printing parameters on the Mode I fracture toughness of polymer bonded joints. The motivation is that realizing small-size, highly optimized AM parts to be later assembled into larger components or on a main structure can be convenient from the manufacturing standpoint, and adhesive bonding is a suitable joining technology as it avoids distortion and material modification due to heat like welding, or the presence of fasteners. Since printing parameters can affect surface roughness and wettability, beside adherend strength and stiffness, they can become effective design parameters for bonded joints. Therefore, in this study two different materials frequently used in FFF, PLA and ABS, and three different printing parameters, namely extruder temperature, printing speed and layer thickness, were selected in order to evaluate their influence on roughness, wettability and tensile behaviour of the adherends. A full-factorial Design of Experiment (DoE) was chosen for the study of roughness and wettability that requires a limited sample manufacturing and measurement time, while a Taguchi L9 orthogonal array was selected for the tensile tests, in order to save manufacturing and testing time. The significance and the mutual interactions of printing parameters were identified by

*Corresponding author: alessandro.pirondi@unipr.it

ANalysis Of VAriance (ANOVA). Combinations yielding maximum and minimum values of the output, respectively, were used to produce adherends for Double Cantilever Beam (DCB) joints and evaluate the effect on Mode I fracture toughness, demonstrating that process parameters do have an effect on fracture toughness and that an optimum value can be found by simply operating on the FFF printer setup.

Keywords: adhesive bonding; additive manufacturing; fused filament fabrication; surface roughness; wettability; fracture toughness; surface modification;

1. Introduction

Engineering relevance of additive manufacturing (AM) is increasing due to process and materials developments that are enabling to obtain components able to withstand loads in structural applications [1]. The modern 3D printers are capable of resolutions up to the μm scale and can be equipped with tools for multi material AM (MMAM), liquid processing, i.e. Liquid Deposition Modelling (LDM), or reinforced materials processing, as long fibre reinforced materials for enhance mechanical properties [2] or conductive whiskers to modify physical properties [3]. Studies on Design for Additive Manufacturing (DfAM) are being carried out to take advantage of the new buildable solutions, as the Functionally Graded Materials (FGM) using MMAM [4], and to explore the actual potentiality of the nominally limitless tailoring of AM. While investigations to further improve the AM processes are being carried out, development of DfAM is pointing out how realizing small-size, highly optimized parts to be later assembled into larger components could be convenient, for example for improving productivity using several 3D printer working in parallel that makes the production process more robust [5].

Therefore, one of the next challenges of DfAM is the definitions of the methods to assemble the AM components together or on a main structure [6], [7]. One of the first investigations on selecting suitable techniques for joining AM components was carried out by Espalin et al. [8], in which methods were sorted in order of effectiveness with respect to the strength of the joint: hot air welding, ultrasonic spot welding, solvent and

adhesive bonding. Adhesive and solvent bonding methods were therefore suggested when one values aesthetic results and is not concerned with mechanical property performance. However, adhesive bonding can be performed without heating, that was proven to have a detrimental effect on the dimensional accuracy of the AM components [9] especially if materials to be joined shows different coefficients of thermal expansion.

Taking advantage of adhesive bonding, heterogeneous materials joints can be performed, Kariz has studied the influence of 3D-printing parameters on the bond shear strength of 3D-printed Acrylonitrile-butadiene-styrene (ABS) copolymer parts bonded to beech wood [10]. After the first work by Arenas et al. [11] in which a method was proposed to select structural adhesives for AM, several works focused on coupling the tailoring enabled by AM to the knowledge of adhesion and failure mechanisms [12] in order to lower peel and shear stress concentrations that develops at the ends of bonded joints, hence to obtain overall joint performance improvements. Examples are FGM adherends obtained in [13] using MMAM, cavities through the thickness of the adherend structures that cause crack trapping [14] or LDM to obtain stepwise adhesive stiffness changes [15]. However, even if improvements in joint strength can be achieved by tailoring methods, most of failures were adhesive, except for epoxy resins that have good compatibility with most of AM materials [16], pointing out that further improvements could be achieved till reaching cohesive or adherend failures.

As remarked by Packham [17] surface physics and morphology plays a key role in the adhesion mechanisms, however only few works are available on surface modifications for AM. Bürenhaus et al [5], Li et al. [18], Fieger et al [19], Leicht et al [20], investigated overlap surface modifications using industrial methods as mechanical abrasion, chemical etching, flame impingement, corona treatment and Atmospheric Pressure Plasma (APP). Even if industrial modifications, and in particular APP, led to adhesion improvements, specific equipment and post-processing are required, thus alternative approaches to embed surface modifications in AM processes were investigated. These approaches do not require any specific equipment and are based on the observations that printing set ups, as parts positioning in the build volume and material deposition patterns, and printing parameters, as layer height, infill, nozzle temperature and speed, affect material physics, i.e. crystallinity [21], and properties, i.e. Young's modulus [22] and surface roughness [23].

Dugbenoo et al. [24] investigated the effect of a surface porosity obtained by controlling though the air gap build parameter. Even if results were outstanding, with

minimum increase in ultimate strength of 145%, a recent work by Bürenhaus et al. [5] outlined that this approach can lead to adherends delamination; this difference in conclusions could be partially justified by the use of different AM processes and materials in this work. Bürenhaus et al. [5] also investigated the effect of the raster angle (material deposition orientation) in respect to the joint loading direction, in order to tailor the adherends surface with micro patterns. Results depicted that surface patterns directionality does not have a relevant effect on joints tensile strength.

In the work of Kovan et al. [25], [26] three different printing orientations together with three different layer thickness combinations were studied using free filament fabrication. The results confirmed that printing parameters do have influence on surface roughness and the authors outlined as general remarks that layer height affect the surface morphology and thus the bonded joints performance, however the correlation is non-linear and changing the build orientation affects also this correlation aside from having high impact on the building time. Finally, it is worth noting that up to date there are no standard testing procedures dedicated to polymeric AM materials and components [27] and some standards, designated for other manufacturing processes, can be used with modifications [28] and should be somehow validated.

As pointed out in the NIST report by Forster [28], at time of writing current standard are not applicable for AM adherends and dedicated modifications are required. Most of the works in literature adopt Single Lap Joints (SLJ). Different geometries have been proposed to investigate additively manufactured joints: Khan et al. modelled the shaft-tube joint [29] while Kovan et al. [26] and Dahmen et al. [30] explored the feasibility of using butt-joint and T-joint testing configurations. Regarding joint characterization, one of the most relevant test methods is DCB as it provides data for mode I loading, which is known to be critical for the strength of adhesive bonding. First explorative works were carried out by Morano et al. [14], [31], Alfano et al. [32], Garcia-Guzman et al. [33]; however, those papers focused on a specific geometrical tailoring across adherend thickness rather than studying if and how AM process parameters could influence the fracture toughness of the joint. A first exploratory work in this sense was done was recently done by the authors [7], showing that FFF setup could affect the strength under Mode I loading. This work is aimed therefore at exploring in detail the influence of the adherend surface and mechanical properties obtained by varying the FFF printing parameters on the Mode I fracture toughness of bonded joints. Two different materials frequently used with FFF, PLA and ABS [34], [35], and three different printing

parameters, namely extruder temperature, printing speed and layer thickness, each at three levels, were selected in order to evaluate their influence on roughness, wettability and mechanical properties of the adherends. This configuration (3 factors, 3 levels) entails 27 possible combinations for each considered material. Parameters values were combined using a statistical approach and their importance and mutual interactions were identified by analysis of variance (ANOVA) [36], [37]. Combinations yielding maximum and minimum values of the output, respectively, were used to produce adherends for Double Cantilever Beam (DCB) joints to assess the effect of the corresponding surface morphologies on Mode-I fracture toughness.

2. Design of Experiment on printing parameters relevant to bonded joint performance

Adhesion mechanisms are based on mechanical interlocking and on the ability of the adhesives to be in contact and interact with the adherends, i.e. wettability and diffusion. In this sense, layer height is a relevant printing parameter as it modifies the surface roughness and affects adhesion trough mechanical interlocking mechanism. Wettability is affected not only by roughness [38] but also by the physics of the surface, i.e. polarity and crystallinity, therefore extruder temperature and deposition speed are relevant parameters for adhesion, too, since they not only affects the surface morphology but also its physics though the thermal cycle experienced by the polymeric material [21], [39], [40]. These printing parameters (extruder temperature, deposition speed and layer height) affect also other mechanical properties and build time. Moreover, interaction exists between parameters, making crucial to evaluate the process parameters-surface properties relationship in order to obtain the desired bonded joint performance improvement.

Samples were manufactured using a fused filament fabrication (FFF) Delta Wasp 4070 3D printer (WASP, Massa Lombarda, Italy, Figure 1) with PLA from BQ (BQ, Madrid, Spain) and ABS from Sienoc. The same flatwise positioning at build plate centre, where temperature is monitored by a thermocouple, was adopted. Preliminary samples were manufactured in order to validate qualitatively this build approach, as these two polymers have different physical properties [41]. The effects of the three design parameters, namely deposition speed (*V*), extruder temperature (*T*) and layer height (*H*), were investigated on three levels, minimum, medium and maximum of the operating ranges (Table 1) indicated by the material suppliers.

Figure 1. Delta Wasp 4070 FFF machine.

Table 1. Printing parameters for PLA and ABS, their levels and coding: note the only values changing between the two materials are printing temperatures.

		PLA	ABS	
Deposition speed, V (mm/s)	**Layer height, H** (mm)	**Extruder temp., T** (°C)	**Extruder temp., T** (°C)	**Taguchi L9 OA DoE coding**
30	0.1	200	230	1
75	0.2	215	240	2
120	0.3	230	250	3

In order to determine how the factors (extruder temperature, deposition speed and layer height) affect the response variables (the mechanical and surface properties), a Design of Experiment (DoE) systematic approach to process optimization [37], [42] has been used. To study the effect of the print parameters on tensile behaviour of the adherends, a Taguchi L_9 Orthogonal Array (OA) [43] was selected instead of a full-factorial one in order to reduce the number of samples to be manufactured, while at the same time the orthogonality of the design allows to apply consistently ANOVA to estimate the effects of each factor and identify its interactions [42]. Printing parameters *V, T, H* are respectively assigned as first, second and third factor of the OA. Since the FFF manufactured PLA and ABS behave almost linearly up to failure, only the ultimate strength has been chosen to represent the tensile behaviour for the sake of simplicity. In

order to have sufficient degrees of freedom (the minimum number of independent experiments to be conducted: one for the mean value and two for each of the remaining factors), the Taguchi L_9 OA is filled in with the nine experiment configurations reported in Table 2. Three repetitions for each configuration have been performed.

Table 2. Coded Taguchi L_9 Orthogonal Array for the characterization of the tensile behaviour of the adherends.

Trial number	**Deposition speed, V** (mm/s)	**Extruder temp., T** (°C)	**Layer height, H** (mm)
L_{9_C1}	1	1	1
L_{9_C2}	1	2	2
L_{9_C3}	1	3	3
L_{9_C4}	2	1	2
L_{9_C5}	2	2	3
L_{9_C6}	2	3	1
L_{9_C7}	3	1	3
L_{9_C8}	3	2	1
L_{9_C9}	3	3	2

Since, differently from tensile tests, the samples to investigate surface morphology and wettability required a short manufacturing time, a full-factorial design was used in this case to investigate changes in morphology and wettability. Print positioning on the build plate, infill and raster orientation are kept constant between different designs.

3. Characterization of AM adherend materials

3.1 Tensile strength

Tensile strength has been evaluated using MaCh3D miniaturized testing machine (MaCh3D srl, Parma, Italy) equipped with a 5 kN load cell and the experimental setup reported in Figure 2. Three repetitions for each L9 OA have been tested, both for PLA and ABS, using MaCh3D proprietary tensile test specimen [44], Figure 3.

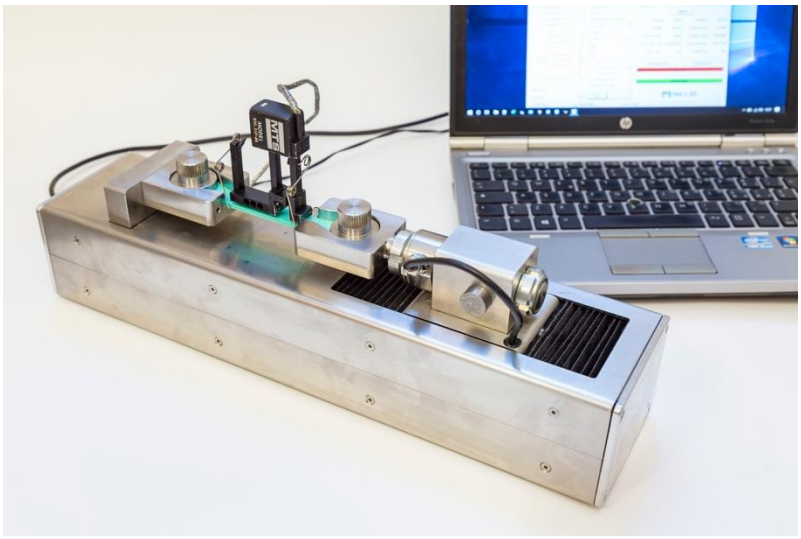

Figure 2. Experimental setup on MaCh3D of tensile testing of adherend materials.

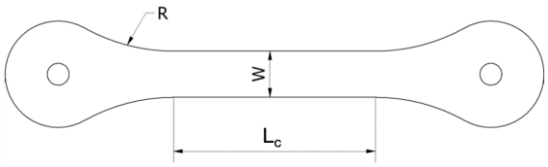

Width, W (mm)	**Reduced sect. , L_c** (mm)	**Shoulder radius, R** (mm)
13	57	52

Figure 3. MaCh3D proprietary tensile test specimen.

Tests were carried out at a constant crosshead speed of 5 mm/min, according to ASTM D638 [45] and a MTS 632 31F-24 extensometer (MTS Systems Corporation, Eden Prairie, USA) was used to measure gauge elongation. Specimens were produced with a 100% infill and a ±45° raster orientation with respect to specimen length direction. The ±45° raster has been adopted for the AM items in this study, since it makes an even surface pattern and it is the standard raster angle assigned by Ultimaker CURA 4.6.1 AM software to the infill of components. Average tensile curves and related scatter bands are reported in Figure 4 (a) for PLA and (b) for ABS, respectively. The legend in Figure 4 reports both the Taguchi L9 OA trial number (see Table 3) and, for the sake of readingness, the corresponding printer setup as V(mm/min)-T(°C)-H(mm).

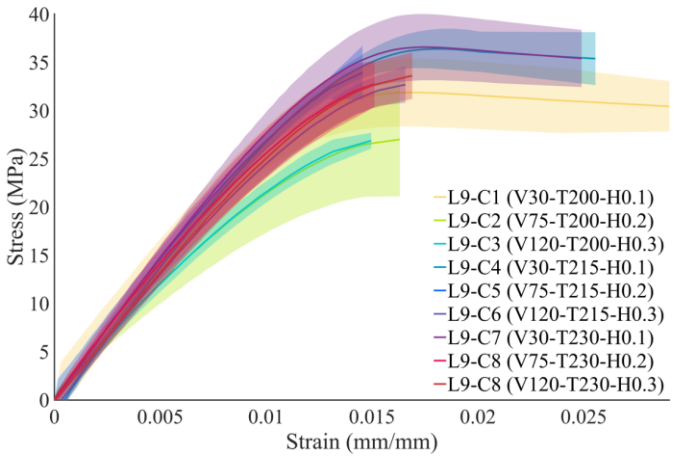

(a)

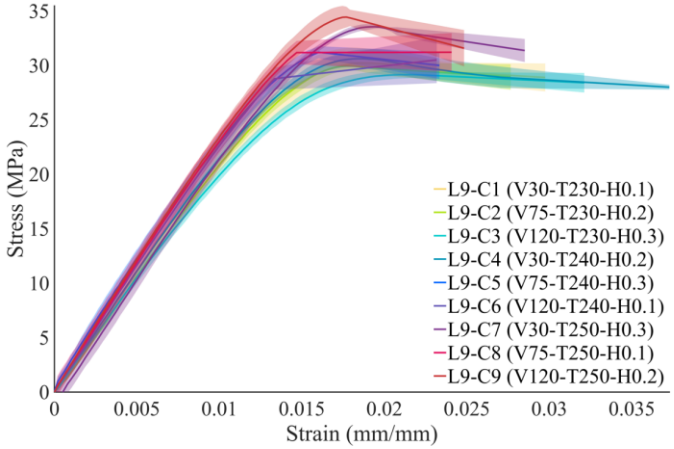

(b)

Figure 4. Averaged strain-stress curves togheter with data dispersion band, for PLA (a) and ABS (b)

Average ultimate tensile strengths (R_m) with error bars representing +/- one standard deviation are reported in Figure 5 for the different set ups chosen according to the Taguchi L_9 OA method.

PLA **ABS**

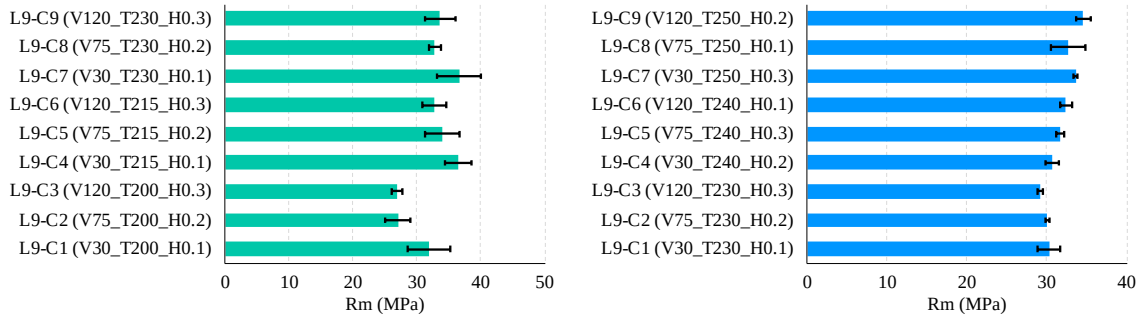

Figure 5. Average ultimate tensile strength (R_m) with error bars representing +/- one standard deviation for the various Taguchi L_9 OA trials.

Regarding R_m, the best mechanical performances are obtained with high extruder temperature for both materials. PLA presents a gradual increase in strength by decreasing layer thickness as well as deposition speed, whilst ABS presents the best performances with high speed and layer thickness, indicating that, in this case, a higher printing temperature seems to be more influential than other parameters. It is confirmed that parameters investigated have a relevant effect on the mechanical properties, maximum variations of R_m are 35% and 19% respectively for PLA and ABS. Similar variations are measured also for Young's modulus average value reported in Figure 6.

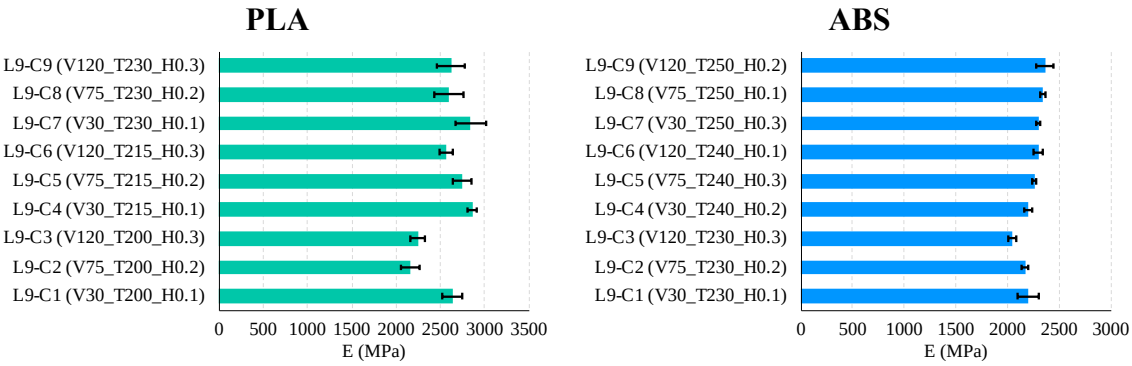

Figure 6. Average Young's modulus (E) with error bars representing +/- one standard deviation for the various Taguchi L_9 OA trials.

3.2 Surface morphology and wettability

One hexahedral tiles of 15×15×1.2 mm^3 size was manufactured for each of the 27

full-factorial set-ups. This small and shallow sample has been adopted in order to save build time, since surface properties and morphology are evaluated only on the last deposited layer and on a 3x3 mm^2 area.

3.2.1 Surface morphology

Changes in morphology of the surface to be bonded are quantified using 2D surface roughness parameter *Sa*, measured according to ISO 25178-2:2012 with a CCI 3D optical profilometer (Taylor Hobson, Leicester, UK). S_a is (Eqn.1) the absolute value of peaks and valleys height, z, integrated along the surface coordinates x and y and averaged over the surface sampling area A:

$$S_a = \frac{1}{A}\iint_A |z(x,y)|\, dxdy \quad (1)$$

The surface is analysed at three different locations on surfaces of 3×3 mm^2 each. *Sa* measurement for each printing set up are reported in Table 4. The configuration "PLA_V120_T200_H0.2" since the measurement was not possible at several points within the sampling area A, as the profile of the valleys was too sharp to be correctly detected by the optical profilometer.

Table 4. Surface roughness values.

PLA

Deposition speed, V (mm/s)	**Extruder temp., T** (°C)	**Layer Height, H** (mm)	**Surface rough., Sa** (μm)
30	200	0.1	**7.97**
		0.2	**9.80**
		0.3	**10.87**
	215	0.1	**7.30**
		0.2	**9.79**
		0.3	**11.06**
	230	0.1	**9.20**
		0.2	**8.16**
		0.3	**11.46**
75	200	0.1	**9.25**
		0.2	**11.17**
		0.3	**11.26**
	215	0.1	**10.61**

ABS

Deposition speed, V (mm/s)	**Extruder temp., T** (°C)	**Layer Height, H** (mm)	**Surface rough., Sa** (μm)
30	230	0.1	**15.35**
		0.2	**12.28**
		0.3	**13.56**
	240	0.1	**17.58**
		0.2	**13.68**
		0.3	**12.87**
	250	0.1	**13.78**
		0.2	**9.53**
		0.3	**19.24**
75	230	0.1	**12.48**
		0.2	**11.81**
		0.3	**14.90**
	240	0.1	**17.13**

		0.2	**8.84**
		0.3	**13.34**
	230	0.1	**11.02**
		0.2	**16.17**
		0.3	**18.68**
120	200	0.1	**23.64**
		0.2	-
		0.3	**15.04**
	215	0.1	**12.64**
		0.2	**15.88**
		0.3	**13.68**
	230	0.1	**12.54**
		0.2	**10.86**
		0.3	**14.24**

		0.2	**11.59**
		0.3	**10.16**
	250	0.1	**11.38**
		0.2	**10.42**
		0.3	**14.81**
120	230	0.1	**13.98**
		0.2	**10.60**
		0.3	**13.52**
	240	0.1	**12.56**
		0.2	**10.88**
		0.3	**15.76**
	250	0.1	**12.07**
		0.2	**11.96**
		0.3	**11.09**

In Figure 7, an example of PLA morphology variation due to a change in the printing parameters is shown.

V: 30 mm/s
T: 200 °C
H: 0.1 mm

V: 30 mm/s
T: 200 °C
H: 0.3 mm

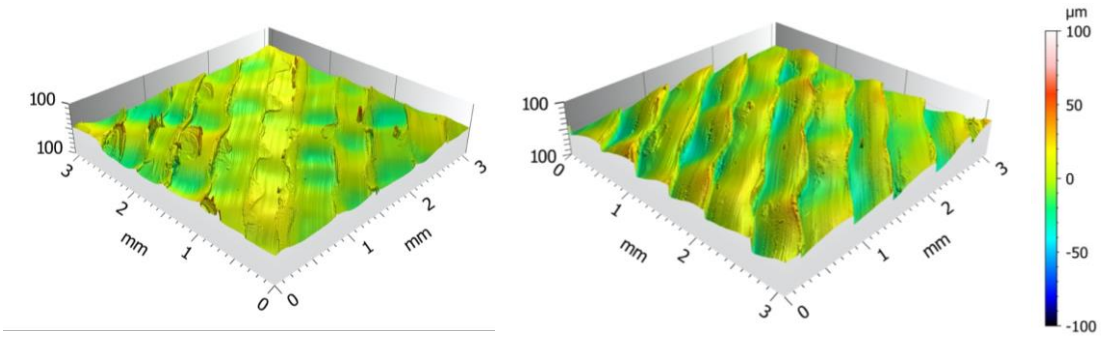

(a) (b)

Figure 7. Comparison between 0.1 mm layer height (a) and 0.3 mm (b) maintaining all other parameters unchanged, in the case of PLA.

3.2.2 Wettability

Wettability analysis was performed on the same tile specimens used for morphology characterization, by the means of sessile drop test with deionised water. The

effect of surface texture direction due to the process was taken in account performing multiple measurements according to the methods proposed in [38] for the experimental investigation of the wettability of rough engineering surfaces. First, the surfaces of the specimens were cleaned using a degreasing solvent (Loctite 7063, Henkel, Milan). Then static contact angle (Θ) measurements were performed at room temperature depositing 2 µl calibrated water drops and taking snapshot after 10 s with a custom-made set-up based on a Dino-lite microscope (AnMo Electronics Corporation, Hsinchu 300, Taiwan) in a direction orthogonal to the surface raster angle. The static contact angle was evaluated from the tangent curve to the drop profile in the contact point between sessile drop and substrate surface. Measurements are repeated 3 times on each tile at 3 different locations. Results are reported in Table 5, respectively.

Table 5. Static contact angle (θ) measurements in the direction orthogonal to the surface raster angle.

PLA

Deposition speed, V (mm/s)	**Extruder temp., T** (°C)	**Layer Height, H** (mm)	**Contact angle., θ** (deg)
30	200	0.1	**61**
		0.2	**66**
		0.3	**77**
	215	0.1	**83**
		0.2	**76**
		0.3	**73**
	230	0.1	**68**
		0.2	**75**
		0.3	**78**
75	200	0.1	**77**
		0.2	**72**
		0.3	**60**
	215	0.1	**78**
		0.2	**65**
		0.3	**78**
	230	0.1	**75**
		0.2	**64**
		0.3	**66**
120	200	0.1	**66**
		0.2	**54**
		0.3	**55**
	215	0.1	**62**
		0.2	**75**
		0.3	**71**
	230	0.1	**65**
		0.2	**67**
		0.3	**73**

ABS

Deposition speed, V (mm/s)	**Extruder temp., T** (°C)	**Layer Height, H** (mm)	**Contact angle., θ** (deg)
30	230	0.1	**64.00**
		0.2	**63.00**
		0.3	**81**
	240	0.1	**82**
		0.2	**81**
		0.3	**77**
	250	0.1	**89**
		0.2	**60**
		0.3	**83**
75	230	0.1	**80**
		0.2	**72**
		0.3	**73**
	240	0.1	**76**
		0.2	**80**
		0.3	**80**
	250	0.1	**81**
		0.2	**80**
		0.3	**85**
120	230	0.1	**83**
		0.2	**71**
		0.3	**71**
	240	0.1	**66**
		0.2	**83**
		0.3	**80**
	250	0.1	**69**
		0.2	**83**
		0.3	**70**

In general, the measured values of static contact angle for the various set ups were slightly different, but comparable, with the ones already published for the investigated materials. Contact angles values maximum variations are 35% for PLA and 39% for ABS. It should be noticed that wettability is a complex phenomenon affected by different phenomena to be taken in account, as roughness that can change wetting regime and surface free energy [38] . As this work is focused on assessing feasibility of using printing parameters to affect bonded joints performance, static contact angle of demineralized water droplets can be used as a qualitative indicator of the sum of these effects. However, after performing more dedicated characterization for a specific material processed with a specific 3D printer, it can be possible to maximize wettability changes.

4. ANOVA for the identification of printing setups of DCB adherends

ANOVA was performed [37] on the data sets from tensile and surface characterizations to identify the main and the interactions effects of printing parameters on tensile strength, roughness and wettability using the procedure validated and presented in [46]. In particular, using the F-ratio test was possible to determine whether factors or interactions were relevant on each variation of the monitored output. If F is higher than a critical value given by the degrees of freedom of the experiment, then the factor or interaction affects the monitored output, otherwise the variation of the monitored output is due to noise. In defining optimised printing parameters for Rm, Sa and Θ, if one of the factor was marked as non-significant, its value was selected as the one minimizing the build time.

4.1 Effect on tensile strength of AM materials

As far as tensile strength (R_m) is concerned, the value at different parameter levels is given in Figure 8 for PLA and in Figure 9 for ABS.

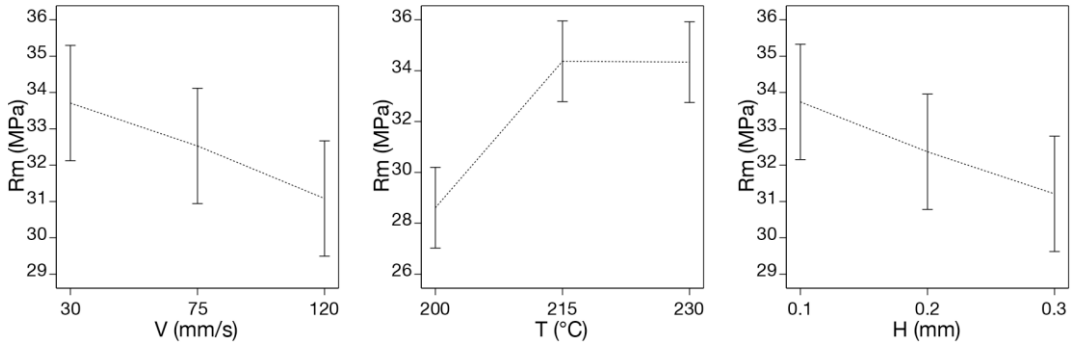

(a) (b) (c)

Figure 8. Main effects for mechanical strength of PLA: Deposition speed (a), Temperature (b), Layer height (c).

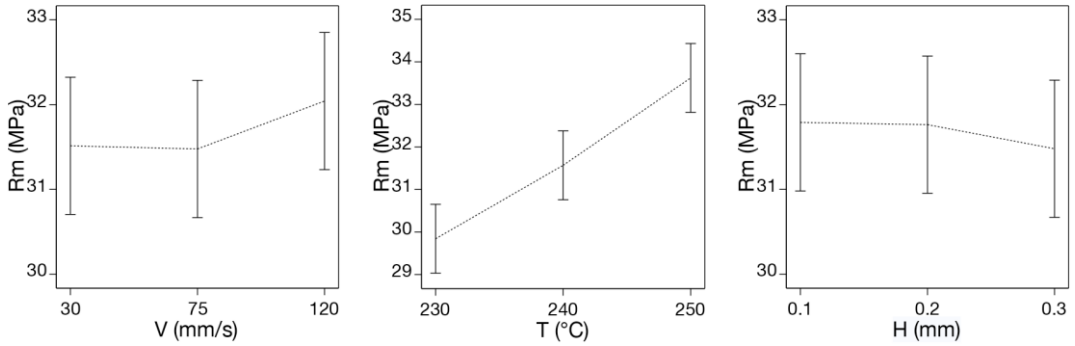

(a) (b) (c)

Figure 9. Main effects for mechanical strength of ABS: Deposition speed (a), Temperature (b), Layer height (c).

The F-test identifies for both materials the extruder temperature as the main effect influencing tensile strength (see Table 6). The Lack-of-Fit F-value of 1.80 (ABS) and 1.93 (PLA) implies that Lack-of-Fit is not significant relative to the pure error, since there is only a 19.33% (ABS) and 17.33% (PLA) chance that a Lack-of-Fit F-value this large could occur due to noise.

Table 6. ANOVA results for tensile strength (R_m).

PLA

Source	F-value	p-value	Significance
Model	4.13	**0.0074**	**significant**

ABS

Source	F-value	p-value	Significance
Model	4.11	**0.0075**	**significant**

T	9.5	**<u>0.0013</u>**	**significant**
V	1.5	0.2482	
H	1.39	0.2732	
Residuals			
Lack-of-Fit	1.8	0.1933	**not significant**

T	11.9	**<u>0.0004</u>**	**significant**
V	0.3327	0.7209	
H	0.0988	0.9064	
Residuals			
Lack-of-Fit	1.93	0.1733	**not significant**

4.2 Effect on surface roughness

Regarding surface roughness in the case of PLA, from one of the most influential effects is deposition speed, having a p-value of 0.0024 (Table 7), as well as the interaction between deposition speed and extruder temperature. Interaction graph for deposition speed and temperature is reported in Figure 10.

Table 7. ANOVA results for surface roughness in the case of PLA adherends.

Source	F-value	p-value	Significance
Model	3.66	**<u>0.0118</u>**	significant
V	9.29	**<u>0.0024</u>**	
T	0.5633	0.5809	
H	1.07	0.3681	
VxT	3.52	**<u>0.0322</u>**	

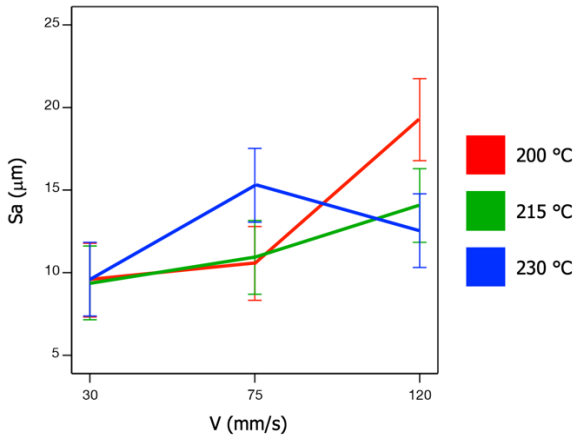

Figure 10. Interaction effect between deposition speed and extruder temperature in determining surface roughness for PLA.

In the case of ABS, the main contribution to surface roughness is determined by layer height, as indicated in Table 8. The model appears to be not significant due to a probability (p-value) higher than 0.05 that F is due to noise. However, looking at the p-values of the single parameters, the origin of such potential noise is related mainly to the extruder temperature, T. A different temperature range and/or a more careful control maybe needed in this case to evaluate if T is effectively influencing the ABS surface roughness. It is worth to remark that, when restricted to V and H only, the model becomes significant.

Table 8. ANOVA results for surface roughness in the case of ABS adherends.

Source	F-value	p-value	Significance
Model	2.22	0.084	not significant
V	1.73	0.2024	
T	0.3925	0.6805	
H	4.53	**0.0239**	

4.3 Effect on wettability

In all cases, a strong interaction exists between all the parameters for both materials as it can be inferred from Table 9 and Table 10 temperature and layer height are the most significant factors.

Table 9. ANOVA results for static contact angle Θ for PLA.

Source	F-value	p-value	Significance
Model	5	**< 0.0001**	significant
V	1.16	0.3208	
T	12.73	**< 0.0001**	
H	12.43	**< 0.0001**	
VxT	0.8679	0.4895	
VxH	3.99	**0.0067**	
TxH	2.26	0.0754	
VxTxH	6.11	**< 0.0001**	

Table 10. ANOVA results for static contact angle Θ for ABS.

Source	F-value	p-value	Significance
Model	6.33	**< 0.0001**	significant
V	2.35	0.1055	
T	8.18	**0.0008**	
H	4.01	**0.0241**	
VxT	4.72	**0.0025**	
VxH	8.56	**< 0.0001**	
TxH	3.42	**0.0149**	
VxTxH	8.58	**< 0.0001**	

4.4 Identification of printing setups for manufacturing of DCB adherends

The results presented in the previous sub-sections are processed to define the printing setups that maximize or minimize the adherend properties relevant for adhesive bonding applications, that is R_m, S_a, Θ. The setups are shown in Table 11 and Table 12 for PLA and ABS, respectively. Some parameters combinations are repeated, hence a reduced number of DCB combinations have been produced, resulting in 4 and 6 different parameters combinations for PLA and ABS, respectively. To facilitate the interpretation of results, a code is provided for each print setup.

Table 11. Printing parameters for PLA adherends.

Parameter	**Roughness**		**Wettability**		**T. Ultimate Strength**	
	MAX	MIN	MAX	MIN	MAX	MIN
Configuration name	*PLA_01*	*PLA_02*	*PLA_02*	*PLA_03*	*PLA_04*	*PLA_03*
Deposition speed, V (mm/s)	120	30	30	120	30	120
Extruder temp., T (°C)	200	215	215	200	230	200
Layer height, H (mm)	0.1	0.1	0.1	0.3	0.1	0.3

Table 12. Printing parameters for ABS adherends.

Parameter	**Roughness**		**Wettability**		**T. Ultimate Strength**	
	MAX	MIN	MAX	MIN	MAX	MIN
Configuration name	*ABS_01*	*ABS_02*	*ABS_03*	*ABS_04*	*ABS_05*	*ABS_06*
Deposition speed, V (mm/s)	30	30	75	30	120	75
Extruder temp., T (°C)	250	250	250	230	250	230
Layer height, H (mm)	0.3	0.2	0.3	0.1	0.1	0.3

5. Double cantilever beam joint testing

5.1 DCB joint design, preparation and testing

A custom DCB specimen geometry has been developed following a DfAM approach [47]. The joint geometry is shown in Figure 11. One of the main constraints was to print adherends with faces to be bonded parallel to the building plane in order to have morphological surface characteristics as close as possible to that analysed during surface characterization. This required the use of support material, removed afterwards, in order to obtain the cylindrical loading hole. Adherends have been printed in pairs, one pair at a time in order to minimize variations due to the different position on the printing table [48], [49].

h (mm)	**B** (mm)	**L** (mm)	**a_0** (mm)	**t** (mm)
10.0	20.0	140.0	30.0	0.3

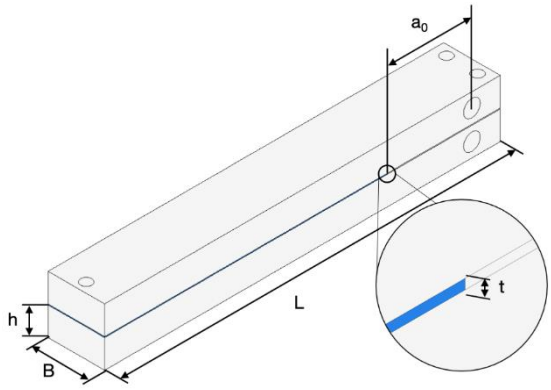

Figure 11. Overall joint geometry.

Figure 12 shows the printing preview of the top view cross section as generated from Ultimaker CURA 4.6.1 software, detailing different structures. In particular, it is possible to see the support structure (light blue) inside the loading hole and the infill reticular structure. Infill shape and percentage influence joint fracture toughness as emerges from the work of Morano et al. [31], [32]. Since the present study of fracture

toughness is comparative, possible differences are eliminated by maintaining the same infill strategy for all specimens. The test setup is shown in Figure 13.

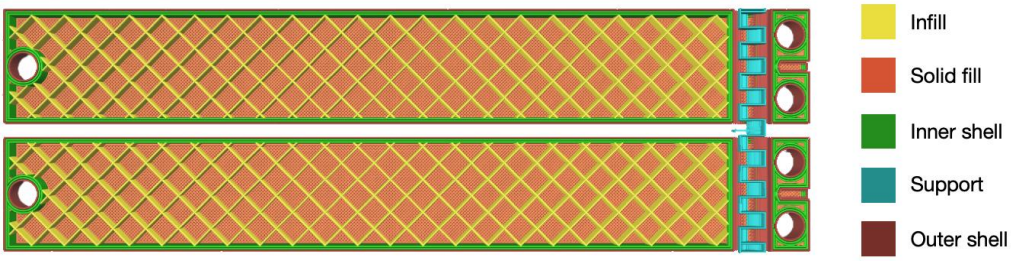

Figure 12. DCB adherends internal structure as previewed from CURA 4.6.1 software.

Figure 13. DCB test setup.

Printing parameters are those reported in Table 11 and Table 12 for PLA and ABS, respectively. Concerning the adhesive, Teroson PU 9225 [50], a polyurethane based two-components adhesive supplied by Henkel that cures at room temperature, was chosen according to the results obtained by Arenas [11]. Bulk tensile properties were characterized by testing ASTM D638 Type IV specimen [45] obtained by pouring adhesive into a Polytetrafluoroethylene (PTFE) mould; results are reported in Table 13.

Table 13. Teroson PU9225 Mechanical properties.

Young's Modulus, E_A (MPa)	**Poisson's Ratio,** υ_A	**Ultimate Strength,** Rm_A (MPa)
576.9	0.33	13.3

Surfaces were cleaned with Loctite 7063 cleaning agent after verifying that the treatment did not affect surface morphology. No mechanical or chemical surface treatment was done in order to preserve the as-built surface texture, with the intention to evaluate if the as-built roughness and texture could compensate by mechanical interlocking the limited adhesion of PLA and ABS, testified by the high surface contact angles. This choice goes into the direction of exploring and exploiting the potential of AM to manufacture ready-to-go components. A polyester sheet was placed on one side of the specimens to create an initial 30 mm long crack (a_0). The adhesive was applied and a layer thickness of 0.3 mm was ensured by placing calibrated metal foils between adherends. The substrates were bonded together by tightening bolts placed in holes at the adherends ends. Joints were cured at room temperature for at least one day before testing. Three repetitions for each combination are performed. A fixture has been developed to allow MaCh3D to perform DCB testing.

5.2 Adherend compliance assessment

For a correct setting and analysis of Mode I DCB fracture test, it is necessary to know how the adherends deform under load. For isotropic materials, the substrate behaviour can be described with a good approximation by the Young's modulus E but this does not apply to anisotropic materials such the ones produced through FFF [35], [51], [52] where out-of-plane elastic modulus and shear modulus play a relevant role in determining

material compliance. Flexural and shear moduli were therefore extracted by three-points bending tests done at different span distances. A three-points bending (3PB) test equipment has been designed to be compliant to ASTM D790 [53] and ASTM D7264 [54], respectively, Figure 14. The test was done for all the setups listed in Table 11 and Table 12.

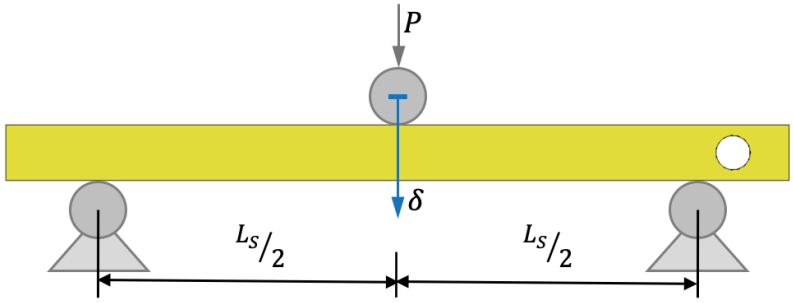

Figure 14. 3PB Test scheme.

The load point displacement, δ, is recorded together with the applied load P. In evaluating specimen compliance, a correction to account for equipment stiffness has been considered. The 3PB specimen compliance, C_{3PB}, is described by Eqn. 2:

$$C_{3PB} = \frac{\delta}{P} = \frac{\left(L_s/2\right)^3}{6E_f I} + 0.6\frac{L_s/2}{GBh} \tag{2}$$

where E_f and G are the flexural modulus and the shear modulus, respectively, and L_s is the span length. Performing tests at different L_s, allows to evaluate E_f and G by best fitting Eqn. 2 with the least squares method, since shear and bending contribution to deformation varies. In particular, four different span lengths from 40 to 100 mm in steps of 20 mm were considered. Tests were performed under displacement control in the elastic regime, where the crosshead speed was being increased for increasing support span in order to keep the same deformation rate. The compliance was evaluated by performing a linear regression on the displacement-load data for each of the tested configurations at every considered span length. For each configuration, two repetitions were performed,

and the average compliance was considered.

The moduli identified are reported in Table 14 for the two materials and the FFF setups listed in Table 11 and Table 12. It is worth to underline that, differently from bulky polymeric components obtained with traditional manufacturing techniques, the shear modulus is more than one order of magnitude lower than the flexural, making the contribution of shear to the bending stiffness non-negligible even for slender structures.

Table 14. Values of E_f and G for the two materials and FFF setups listed in Table 11 and Table 12.

Specimen	E_f (MPa)	G (MPa)	**Correspondance with Table 11 and Table 12**
PLA_01	1608	65	Max. Roughness
PLA_02	1622	181	Min. Roughness, Max. Wettability
PLA_03	1697	114	Min. Wettability, Min. Tensile Strength
PLA_04	1911	80	Max. Tensile Strength
ABS_01	1167	90	Max. Roughness
ABS_02	1493	56	Min. Roughness
ABS_03	1288	65	Max. Wettability
ABS_04	1404	66	Min. Wettability
ABS_05	1495	53	Max. Tensile Strength
ABS_06	1367	51	Min. Tensile Strength

DCB test data reduction method

The testing of a DCB with a relatively soft layer in between the two cantilevers, impose to consider root rotation at the crack tip, stress concentration effects, and the presence of a non-negligible fracture process zone (FPZ) ahead of the crack tip [Chaves et al.], but it requires also that the deformation of the adhesive layer is accounted for in the evaluation of strain energy release rate [Sekiguchi et al.]. Therefore, the method reported in the work of de Moura [15], [55], [56], based on the definition of an equivalent crack length, a_e, evaluated directly from specimen compliance (C, that accounts also for the presence of a at the crack tip. The compliance C is expressed as:

$$C = \frac{8{a_e}^3}{E_f B h^3} + \frac{12 a_e}{5GBh} \tag{3}$$

and can be rewritten in polynomial form [55]:

$$\alpha a_e^3 + \beta a_e \ + \gamma = 0 \tag{4}$$

where the coefficients α, β and γ are, respectively:

$$\alpha = \frac{8}{E_f B h^3} \qquad \beta = \frac{12}{5GBh} \qquad \gamma = -C \tag{5}$$

By solving Eqn. (4) and considering only the real solutions, a_e takes the form:

$$a_e \ = \frac{1}{6\alpha} A - \frac{2\beta}{A} \tag{6}$$

being A:

$$A = \left[\left(-108\gamma + 12\sqrt{3\left(\frac{4\beta^3 + 27\gamma^2\alpha}{\alpha}\right)} \right) \alpha^2 \right]^{\frac{1}{3}} \tag{7}$$

The strain energy release rate becomes then:

$$\mathrm{G}_I = \frac{6P^2}{B^2 h}\left(\frac{2a_e^2}{h^2 E_f} + \frac{1}{5G}\right) \tag{8}$$

The compliance, *C*, is evaluated as the slope dΔ/dP (Δ = crack opening along the load line) recorded in the partial unloadings performed at intervals during the test. Since the unloading, in general, do not point to the origin of the Δ-P diagram because of inelastic phenomena at the crack tip and small adjustments/hysteris in the load train, the simple

ratio Δ/P may not represent correctly the compliance of the joint.

Mode I fracture toughness results

The results are reported in two separate diagrams for PLA and ABS, respectively. In each diagram, every set of data collects the results of the three repetitions. For both materials, failure was always interfacial due to the relatively low wettability and the intentional absence of surface preparation but cleaning (see Sect. 5.1), therefore the surface pattern left by FFF was apparently not able to compensate the inherent low adhesion of these materials, except in the case of PLA_04 where in two out of the three specimens a partly cohesive failure was recorded: example of one of the cohesive rupture is reported in Figure 15.

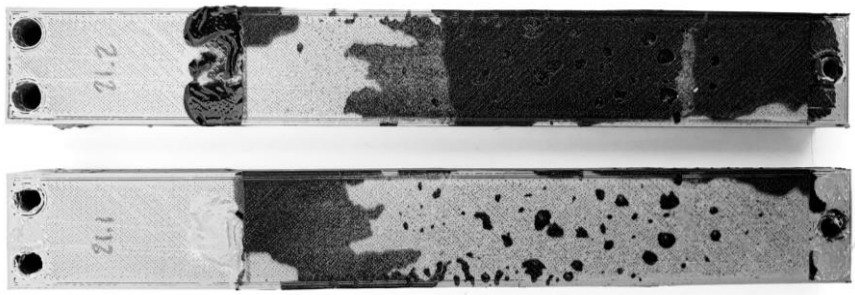

Figure 15. One of the three tested specimens for PLA_04 configuration, showing partially cohesive failure.

Another point common to all experiments is that a more or less steep R-curve was present that does not come to a steady-state value in the range of crack propagation tested. It is possible that the size of the specimen, which was defined according printing chamber size and build time limitations, was not large enough to allow a crack propagation sufficient to reach a plateau of fracture toughness. The discussion can be done therefore only on the slope of the R-curve, with the underlying possibility that a higher slope would lead to a higher steady-state fracture toughness. Results for PLA specimens, reported in Figure 16, show similar value of fracture toughness at the beginning of crack propagation in all cases, while the maximum rate of increase of fracture toughness is obtained with specimen PLA_04 (maximum tensile strength, flexural modulus) whilst PLA_03 (minimum wettability and tensile strength) presents the lowest values. Considering ABS joints, from Figure 17 it can be inferred that all the configurations show both similar

values at the beginning of propagation and the R-curve slopes are not much different from each other, giving in fact a unique, large scatter band that is, ABS joints fracture toughness is little influenced by printer setup. Looking more closely at the linear regression of the single configurations, one can say a higher G_{IC} corresponds to ABS_01 and ABS_06 (the two configurations with the highest values of roughness) while ABS_04 (minimum wettability) present instead the lower values. This means that, alike for PLA, wettability must be maximized but the roughness seems also to play some role in this case, though the large scatter cannot afford a definitive conclusion about this point.

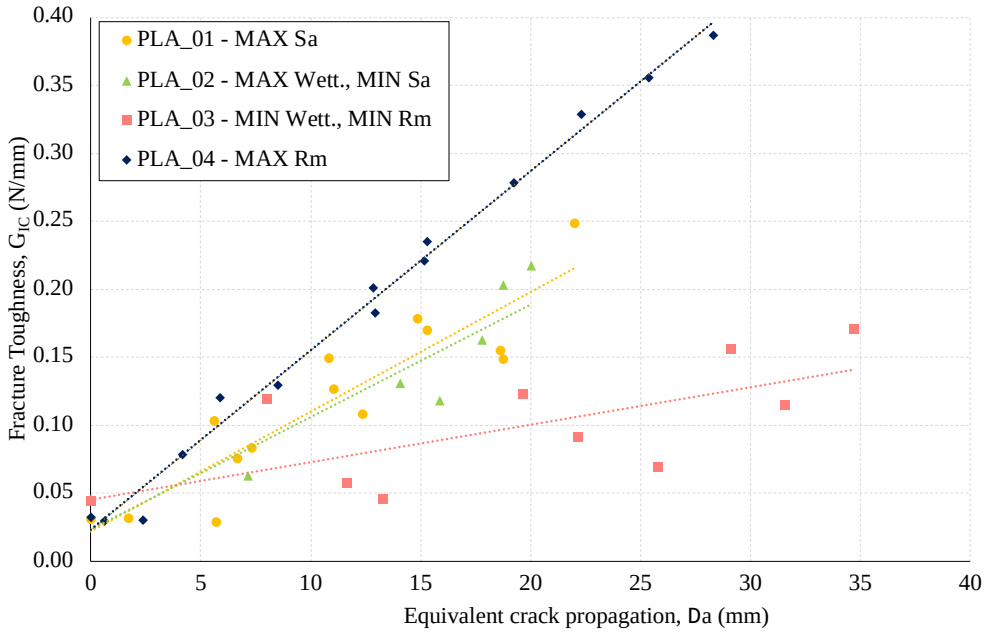

Figure 16. Fracture toughness values for PLA adherends.

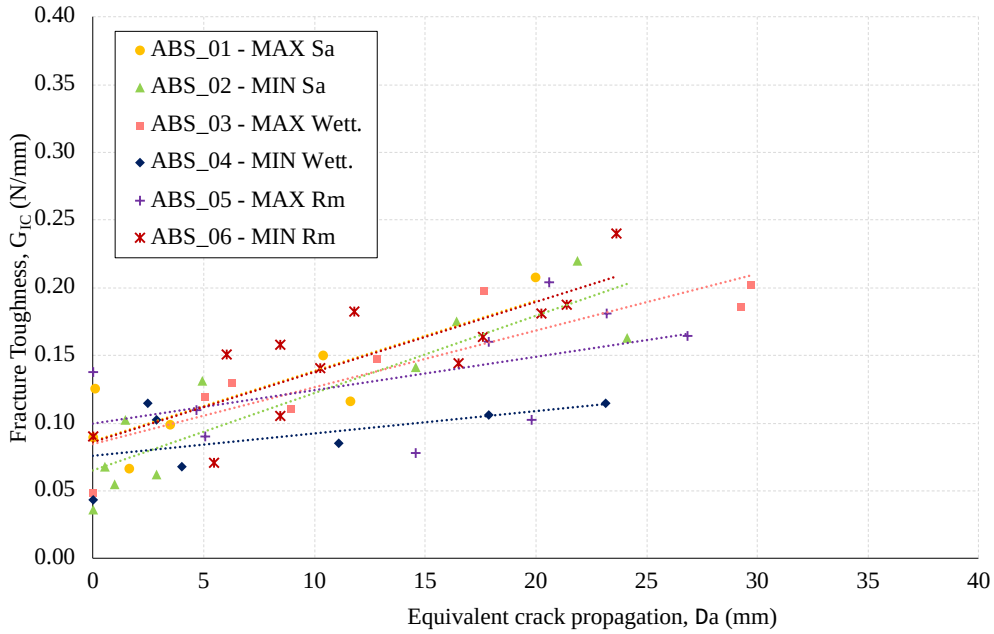

Figure 17. Fracture toughness values for ABS adherends.

In order to prove if the R-curve behaviour is typical of this adhesive or if it is related to the FFF parameters, comparative tests have been carried out using aluminium adherends and the same polyurethane adhesive as in the case of FFF joints. The geometry used is the same described in the work of [57]. Adherends were simply grit-blasted and cleaned with Loctite 7063. Adhesive thickness has been kept at 0.3mm as in FFF joints by means of calibrated foils. Three repetition were performed. Failure was cohesive in thsi case and fracture toughness values are reported in Figure 18.

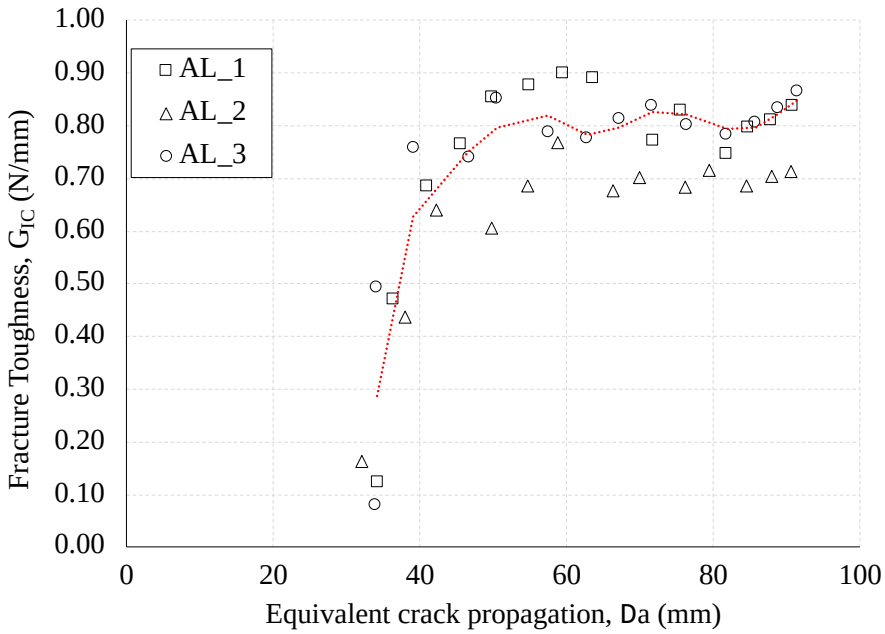

Figure 18. Fracture toughness values for aluminium adherends.

As it can be seen, an R-curve develops also in this case but much steeper than with FFF polymeric adherends. In fact, G_{IC} stabilizes around 0.8 N/mm after about 20 mm of crack propagation, while in the case of ABS and PLA it did not grow above 0.4 N/mm. It is worth to underline that the value of G_{IC} obtained with tests on aluminum joints are well in agreement with those in the work of Boutar et al. [57]. The adhesive shows therefore an inherent R-curve behaviour that, in the case of FFF joints, may be more or less pronounced depending on manufacturing parameters, that is these latter become indeed joint design parameters.

Conclusions

This work explored the influence of the adherends surface and strength/stiffness characteristics obtained by varying the FFF printing parameters, namely extruder temperature, deposition speed and layer thickness, on the Mode I fracture toughness of bonded joints of two different materials frequently used in FFF, PLA and ABS, respectively. Combinations of parameters giving maximum and minimum values of the surface roughness, respectively, wettability and tensile strength of the adherends were used to manufacture samples for Double Cantilever Beam (DCB) joints. For both

materials, failure was found to be interfacial, meaning that the surface pattern left by FFF could not compensate the inherent low adhesion except in one case (PLA with maximum tensile strength), where two out of the three specimens exhibited a partly cohesive failure. All experiments were characterized by a more or less steep R-curve that does not come to a steady-state value in the range of crack propagation tested. A conclusion can be therefore drawn only on the slope of the R-curve, with the underlying possibility that a higher slope would lead to a higher steady-state fracture toughness. Under these conditions, in the case of PLA, a noticeable dependence on the printing parameters was found, where the strength (stiffness) and the wettability are most influential. In the case of ABS instead, it was much more difficult to distinguish a trend since the results of the experiments seem to fall into a unique, large scatter band. However, zooming on the values of each test, again wettability has to be maximized but the roughness seems also to play a role for this material. For both materials, the joints showed a positive dependence of fracture toughness on crack growth (R-curve), that is more pronounced in the case of PLA. The development of a R-curve has been proven to be characteristic of the adhesive used in this work and not simply related to the surface morphology of the adherends, since it was found also by testing DCB joints with aluminium adherends. However, since for PLA or ABS adherends the R-curve resulted more or less steep depending on the printing parameters, it can be concluded that FFF parameters are indeed bonded joint design factors. This conclusion adds a new aspect to the design of bonded joints of polymeric FFF adherends. In fact, most works in the literature used AM to shape or give a stiffness gradation to the adherends in order to improve the strength; this however requires in general a non-trivial numerical study, special printers and a complicated setup. In the present study it is shown instead that an improvement can also be found by simply operating on the setup of a common FFF printer.

References

[1] M. H. Ali, S. Batai, and D. Sarbassov, ‘3D printing: a critical review of current development and future prospects’, *Rapid Prototyping Journal*, 2019.

[2] D. Zindani and K. Kumar, ‘An insight into additive manufacturing of fiber reinforced polymer composite’, *International Journal of Lightweight Materials and Manufacture*, vol. 2, no. 4, pp. 267–278, 2019.

[3] D. J. Horst and P. P. A. Junior, ‘3D-Printed Conductive Filaments Based on Carbon Nanostructures Embedded in a Polymer Matrix: A Review’, *International Journal of Applied Nanotechnology Research (IJANR)*, vol. 4, no. 1, pp. 26–40, 2019.

[4] G. H. Loh, E. Pei, D. Harrison, and M. D. Monzon, 'An overview of functionally graded additive manufacturing', *Additive Manufacturing*, vol. 23, pp. 34–44, 2018.

[5] F. Bürenhaus, E. Moritzer, and A. Hirsch, 'Adhesive bonding of FDM-manufactured parts made of ULTEM 9085 considering surface treatment, surface structure, and joint design', *Welding in the World*, vol. 63, no. 6, pp. 1819–1832, 2019.

[6] M. Frascio, E. A. de S. Marques, R. J. C. Carbas, L. F. M. da Silva, M. Monti, and M. Avalle, 'Review of Tailoring Methods for Joints with Additively Manufactured Adherends and Adhesives', *Materials*, vol. 13, no. 18, p. 3949, Sep. 2020, doi: 10/ghd26h.

[7] L. Bergonzi, M. Frascio, M. Vettori, F. Moroni, A. Pirondi, and M. Avalle, 'Evaluation of surface roughness influence on the strength of structural adhesive joints between additively manufactured adherends', presented at the ESIAM19, Trondheim, Sep. 2019.

[8] D. Espalin *et al.*, 'Analysis of bonding methods for FDM-manufactured parts', in *21st Annual International Solid Freeform Fabrication Symposium-An Additive Manufacturing Conference*, 2010, pp. 37–47.

[9] J. Butt and R. Bhaskar, 'Investigating the Effects of Annealing on the Mechanical Properties of FFF-Printed Thermoplastics', *Journal of Manufacturing and Materials Processing*, vol. 4, no. 2, p. 38, 2020.

[10] M. Kariz, M. K. Kuzman, and M. Sernek, 'Adhesive bonding of 3D-printed ABS parts and wood', *Journal of Adhesion Science and Technology*, vol. 31, no. 15, pp. 1683–1690, Aug. 2017, doi: 10.1080/01694243.2016.1268414.

[11] J. M. Arenas, C. Alía, F. Blaya, and A. Sanz, 'Multi-criteria selection of structural adhesives to bond ABS parts obtained by rapid prototyping', *International Journal of Adhesion and Adhesives*, vol. 33, pp. 67–74, Mar. 2012, doi: 10.1016/j.ijadhadh.2011.11.005.

[12] L. F. Silva, 'Design rules and methods to improve joint strength', in *Handbook of adhesion technology*, 2011.

[13] J. Ubaid, B. L. Wardle, and S. Kumar, 'Strength and Performance Enhancement of Multilayers by Spatial Tailoring of Adherend Compliance and Morphology via Multimaterial Jetting Additive Manufacturing', *Sci Rep*, vol. 8, no. 1, p. 13592, Dec. 2018, doi: 10/gd9vbg.

[14] C. Morano, P. Zavattieri, and M. Alfano, 'Tuning energy dissipation in damage tolerant bio-inspired interfaces', *Journal of the Mechanics and Physics of Solids*, p. 103965, 2020, doi: 10/gg6msf.

[15] Y. Sekiguchi, M. Nakanouchi, K. Haraga, I. Takasaki, and C. Sato, 'Experimental investigation on strength of stepwise tailored single lap adhesive joint using second-generation acrylic adhesive via shear and low-cycle shear tests', *International Journal of Adhesion and Adhesives*, vol. 95, p. 102438, 2019, doi: 10/gg6msg.

[16] A. Spaggiari and F. Denti, 'Mechanical strength of adhesively bonded joints using polymeric additive manufacturing', *Proceedings of the Institution of Mechanical Engineers, Part C: Journal of Mechanical Engineering Science*, p. 095440621985022, 2019, doi: 10.1177/0954406219850221.

[17] D. E. Packham, *Theories of fundamental adhesion*. ed: Springer Berlin Heidelberg, 2011.

[18] W. Li, L. Sang, X. Jian, and J. Wang, 'Influence of sanding and plasma treatment on shear bond strength of 3D-printed PEI, PEEK and PEEK/CF', *International Journal of Adhesion and Adhesives*, p. 102614, 2020, doi: 10/gg6msm.

[19] T. Fieger, D. Nugara, J. Huebner, and G. Witt, ‘Optimization of adhesively joined laser-sintered parts’, in *Proceedings of the 28th Annual International Solid Freeform Fabrication Symposium*, 2017, pp. 567–577.

[20] H. Leicht *et al.*, ‘Adhesive bonding of 3D-printed plastic components’, *The Journal of Adhesion*, vol. 96, no. 1–4, pp. 48–63, 2020, doi: 10/gg6msn.

[21] Y. Liao *et al.*, ‘Effect of porosity and crystallinity on 3D printed PLA properties’, *Polymers*, vol. 11, no. 9, p. 1487, 2019, doi: 10/gg6mss.

[22] V. E. Kuznetsov, A. N. Solonin, A. Tavitov, O. Urzhumtsev, and A. Vakulik, ‘Increasing strength of FFF three-dimensional printed parts by influencing on temperature-related parameters of the process’, *Rapid Prototyping Journal*, 2020, doi: 10/gg6n24.

[23] K. Kandananond, ‘Optimization of fused filament fabrication system by response surface method’, *International Journal of Metrology and Quality Engineering*, vol. 11, p. 4, 2020.

[24] E. Dugbenoo, M. F. Arif, B. L. Wardle, and S. Kumar, ‘Enhanced Bonding via Additive Manufacturing-Enabled Surface Tailoring of 3D Printed Continuous-Fiber Composites’, *Adv. Eng. Mater.*, vol. 20, no. 12, p. 1800691, Dec. 2018, doi: 10.1002/adem.201800691.

[25] V. Kovan, G. Altan, and E. S. Topal, ‘Effect of layer thickness and print orientation on strength of 3D printed and adhesively bonded single lap joints’, *J Mech Sci Technol*, vol. 31, no. 5, pp. 2197–2201, May 2017, doi: 10/gbgxv3.

[26] V. Kovan, G. Altan, E. S. Topal, and H. E. Camurlu, ‘Surface Roughness Effect on the 3d Printed Butt Joints Strength’, *International Scientific Conference BALTTRIB*, vol. 0, no. 0, pp. 117-121–121, Feb. 2016.

[27] J. R. C. Dizon, A. H. Espera, Q. Chen, and R. C. Advincula, ‘Mechanical characterization of 3D-printed polymers’, *Additive Manufacturing*, vol. 20, pp. 44–67, Mar. 2018, doi: 10.1016/j.addma.2017.12.002.

[28] A. M. Forster, ‘Materials Testing Standards for Additive Manufacturing of Polymer Materials: State of the Art and Standards Applicability’, National Institute of Standards and Technology, NIST IR 8059, May 2015. doi: 10.6028/NIST.IR.8059.

[29] M. A. Khan, S. Kumar, and W. J. Cantwell, ‘Additively manufactured cylindrical systems with stiffness-tailored interface: Modeling and experiments’, *International Journal of Solids and Structures*, vol. 152–153, pp. 71–84, Nov. 2018, doi: 10/gfjrjp.

[30] V. Dahmen, A. J. Redmann, J. Austermann, A. L. Quintanilla, S. J. Mecham, and T. A. Osswald, ‘Fabrication of hybrid composite T-joints by co-curing with 3D printed dual cure epoxy’, *Composites Part B: Engineering*, vol. 183, p. 107728, Feb. 2020, doi: 10/gg646d.

[31] C. Morano, L. Bruno, L. Pagnotta, and M. Alfano, ‘Analysis of crack trapping in 3D printed bio-inspired structural interfaces’, *Procedia Structural Integrity*, vol. 12, pp. 561–566, Jan. 2018, doi: 10.1016/j.prostr.2018.11.063.

[32] M. Alfano, C. Morano, L. Bruno, M. Muzzupappa, and L. Pagnotta, ‘Analysis of debonding in bio-inspired interfaces obtained by additive manufacturing’, *Procedia Structural Integrity*, vol. 8, pp. 604–609, Jan. 2018, doi: 10.1016/j.prostr.2017.12.059.

[33] L. García-Guzmán, L. Távara, J. Reinoso, J. Justo, and F. París, ‘Fracture resistance of 3D printed adhesively bonded DCB composite specimens using structured interfaces: Experimental and theoretical study’, *Composite Structures*, vol. 188, pp. 173–184, 2018, doi: 10/gc33ck.

[34] ‘FDM 3D Printing materials compared’, *3D Hubs*. https://www.3dhubs.com/knowledge-base/fdm-3d-printing-materials-compared (accessed May 11, 2019).

[35] D. Popescu, A. Zapciu, C. Amza, F. Baciu, and R. Marinescu, 'FDM process parameters influence over the mechanical properties of polymer specimens: A review', *Polymer Testing*, vol. 69, pp. 157–166, Aug. 2018, doi: 10/gd5kvc.

[36] B. M. Gopalsamy, B. Mondal, and S. Ghosh, 'Taguchi method and ANOVA: An approach for process parameters optimization of hard machining while machining hardened steel', vol. 68, p. 10, 2009.

[37] D. C. Montgomery, *Design and Analysis of Experiments*. John Wiley & Sons, 2017.

[38] K. J. Kubiak, M. C. T. Wilson, T. G. Mathia, and Ph. Carval, 'Wettability versus roughness of engineering surfaces', *Wear*, vol. 271, no. 3–4, pp. 523–528, Jun. 2011, doi: 10.1016/j.wear.2010.03.029.

[39] D. Vaes, M. Coppens, B. Goderis, W. Zoetelief, and P. Van Puyvelde, 'Assessment of crystallinity development during fused filament fabrication through fast scanning chip calorimetry', *Applied Sciences*, vol. 9, no. 13, p. 2676, 2019, doi: 10/gg6msq.

[40] V. Srinivas, C. S. J. van Hooy-Corstjens, and J. A. W. Harings, 'Correlating molecular and crystallization dynamics to macroscopic fusion and thermodynamic stability in fused deposition modeling; a model study on polylactides', *Polymer*, vol. 142, pp. 348–355, Apr. 2018, doi: 10/gdgnmr.

[41] T. A. Osswald, E. Baur, and N. Rudolph, *Plastics Handbook: The Resource for Plastics Engineers*. Carl Hanser Verlag GmbH Co KG, 2019.

[42] J. Antony and M. Kaye, *Experimental quality: a strategic approach to achieve and improve quality*. Springer Science & Business Media, 2012.

[43] G. Taguchi, S. Konishi, and S. Konishi, *Taguchi Methods: Orthogonal Arrays and Linear Graphs. Tools for Quality Engineering*. American Supplier Institute Dearborn, MI, 1987.

[44] L. Bergonzi, M. Vettori, A. Pirondi, F. Moroni, and F. Musiari, 'Numerical and experimental validation of a non-standard specimen for uniaxial tensile test', *Procedia Structural Integrity*, vol. 12, pp. 392–403, 2018, doi: 10.1016/j.prostr.2018.11.078.

[45] ASTM D638-14, *Standard Test Method for Tensile Properties of Plastics*. West Conshohocken, PA: ASTM International, 2014.

[46] M. Frascio *et al.*, 'Additive manufacturing process parameter influence on mechanical strength of adhesive joints, preliminary activities', *APP*, vol. 25, pp. 41–47, Dec. 2019, doi: 10/ggtss6.

[47] M. K. Thompson *et al.*, 'Design for Additive Manufacturing: Trends, opportunities, considerations, and constraints', *CIRP annals*, vol. 65, no. 2, pp. 737–760, 2016, doi: 10/f85q6d.

[48] J. W. Frascati, 'Effects Of Position, Orientation, And Infiltrating Material On Three Dimensional Printing Models', p. 65.

[49] I. Gajdoš and J. Slota, 'Influence of printing conditions on structure in FDM prototypes', *Technical Gazette*, vol. 20, no. 2, pp. 231–236, 2013.

[50] Henkel, *TEROSON PU 9225 Technical Data Sheet*. Henkel AG & Co. KGaA, 2017.

[51] S. Ahn, M. Montero, D. Odell, S. Roundy, and P. K. Wright, 'Anisotropic material properties of fused deposition modeling ABS', *Rapid Prototyping Journal*, vol. 8, no. 4, pp. 248–257, Oct. 2002, doi: 10.1108/13552540210441166.

[52] L. Warnung, S.-J. Estermann, and A. Reisinger, 'Mechanical Properties of Fused Deposition Modeling (FDM) 3D Printing Materials', *RTejournal - Fachforum für Rapid Technologien*, vol. 2018, no. 1, Dec. 2018, [Online]. Available: http://www.rtejournal.de/ausgabe-15-2018/4781.

[53] ASTM D790-17, *Standard Test Methods for Flexural Properties of Unreinforced and Reinforced Plastics and Electrical Insulating Materials*. West Conshohocken, PA: ASTM International, 2017.

[54] ASTM D 7264/D 7264M – 07, *Standard Test Method for Flexural Properties of Polymer Matrix Composite Materials*. 2007.

[55] M. F. S. F. de Moura, J. J. L. Morais, and N. Dourado, 'A new data reduction scheme for mode I wood fracture characterization using the double cantilever beam test', *Engineering Fracture Mechanics*, vol. 75, no. 13, pp. 3852–3865, Sep. 2008, doi: 10/cc7k28.

[56] F. J. P. Chaves, L. F. M. da Silva, M. F. S. F. de Moura, D. A. Dillard, and V. H. C. Esteves, 'Fracture Mechanics Tests in Adhesively Bonded Joints: A Literature Review', *The Journal of Adhesion*, vol. 90, no. 12, pp. 955–992, Nov. 2014, doi: 10/gf75zz.

[57] Y. Boutar, S. Naïmi, T. Daami, S. Mezlini, L. F. M. da Silva, and M. B. S. Ali, 'Mode I Fracture Energy of One-Component Polyurethane Adhesive Joints as Function of Bond Thickness for the Automotive Industry', in *Design and Modeling of Mechanical Systems—III*, M. Haddar, F. Chaari, A. Benamara, M. Chouchane, C. Karra, and N. Aifaoui, Eds. Cham: Springer International Publishing, 2018, pp. 393–403.